2005 American Control Conference
June 8-10, 2005. Portland, OR, USA

Control of Thermal Ignition in Gasoline Engines

C. J. Chiang and A. G. Stefanopoulou
University of Michigan, Ann Arbor
Email: cjchiang, annastef@umich.edu

Abstract— **In this paper a model based controller is designed to regulate the crank angle of 50% fuel burned (CA50) and the air to fuel ratio (AFR) in the exhaust manifold of a gasoline engine during fuel step changes. The regulation of the combustion timing is based on manipulating the charge temperature through the internal and external dilutions which are achieved by controlling the lift of a secondary opening of the exhaust valve, also known as Rebreathing Lift (RBL), and the Exhaust Gas Recirculation (EGR) valve. The paper includes a brief introduction of the engine model followed by its experimental validation during fuel step changes which are considered as disturbances for the control problem. A two-input two-output controller is designed for the linearized model and simulations of closed loop response with the controller applied to the nonlinear model are presented. Finally, an equivalent reduced order controller is derived to facilitate implementation on a dynamometer facility.**

I. Introduction

Control of the combustion timing through the thermal management of cylinder charge is shown in this paper. The resulting thermal ignition (TI) engine, also known as homogeneous charge compression ignition (HCCI) engine, is fundamentally different from the spark ignition (SI) and the compression ignition (CI) engines. In the TI engines the combustion initiation depends on kinetically driven oxidation process [1] that does not rely on flame propagation [2]. The TI engines have (i) high fuel efficiency due to unthrottled operation and rapid heat release and (ii) low emissions of nitrogen oxides due to the low peak cylinder temperatures. Lean mixtures (AFR=20) allow operation with conventional catalytic converters for reduction of hydrocarbons and other emissions through exhaust aftertreatment.

Methods for controlling combustion phasing include intake air temperature modulation [3], variable compression ratio [4], water injection [5], mass flow ratio of two fuel types [6], [7], exhaust throttling [8], and variable valve timing [9]. All the above approaches require novel actuation mechanisms, so the hardware development imposes additional control challenges that might eventually determine the commercial success of each approach. Apart from the hardware requirements, early work showed that the combustion initiation is very sensitive to the charge temperature at intake valve closing (IVC) [10], [11]. Consequently, the ignition timing can only be indirectly controlled through the slow and complex thermal management of the cylinder charge, instead of the fast and direct actuation of the spark discharge or the fuel injection timing that are used to initiate combustion in SI and CI engines, respectively [5].

In this paper we consider a variable exhaust valve actuation similar to the one in [9]. Specifically, the lift of a second exhaust valve opening that occurs during the intake stroke is used to control the charge dilution. We refer to this actuator as rebreathing lift (RBL) and we assume continuous control of the lift as shown in Fig. 1. Conventional exhaust gas recirculation (EGR) valve controls the burned gas fraction in the intake manifold. The EGR flow is mixed with the fresh air and passes through a heat exchanger (HEX) that controls the inlet manifold temperature at 90^o C. Coordination of RBL and EGR allows regulation of (i) the combustion timing through management of the hot and cold dilution in the cylinder and (ii) the AFR in the exhaust manifold for catalyst after-treatment. We assume cycle-to-cycle measurement of the crankangle where 50% of fuel is burned (CA50). This crankangle is typically located near the location of peak cylinder pressure (LPP) that can be inferred through cylinder pressure measurements. We also assume fast measurements of AFR in the exhaust manifold. We neglect the dynamics of the physical actuation for RBL and EGR, by assuming that the actual lift in RBL and open area in EGR are achieved instantaneously after issued by the controller. We also assume that the engine speed and fuel flow rate are measured disturbances. We first synthesize and design a multivariable controller for RBL and EGR that regulates combustion phasing (CA50) and AFR during changes in fueling level. The controller is then simplified to a dynamic feedforward and decentralized feedback controllers that can be tuned on-line. The controller is developed based on a control oriented model [12] that captures the HCCI combustion and realistic manifold flow, pressure, and temperature dynamics. The controller tuning takes into account the local and global dynamic characteristics including stability properties for the system ([13]).

II. Model

The model we use in this control study is based on the mean value model constructed in [12] where the cylinder is modeled as a pump based on cycle-average cylinder flows. Flows from volume x to volume y are denoted as W_{xy}. The fueling level is denoted as W_f. The subscript c is used to denote variables associated with the cylinder, and er is used for the exhaust runner. The subscript 1 denotes the intake manifold variables, 2 is used for exhaust manifold variables, and 0 is used for atmospheric conditions.

This original mean value model in [12] has 8 states: two states in the intake manifold, mass m_1 and burned

0-7803-9098-9/05/$25.00 ©2005 AACC

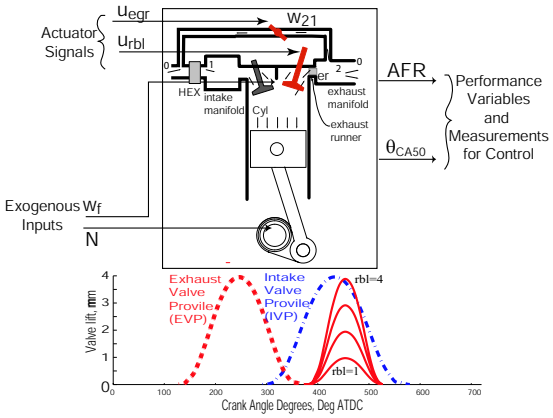

Fig. 1. Schematic representation of the engine with basic input-output signal description for the control problem.

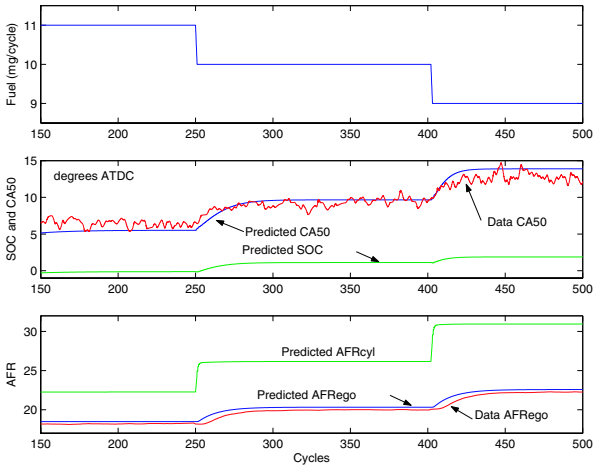

Fig. 2. Fuel step response validation.

gas fraction b_1; three states in the exhaust manifold, mass m_2, burned gas fraction b_2 and pressure p_2; three states from the unit delay, the effective average mass flow rate that flows from the cylinder through the exhaust runner to the exhaust manifold W_{c2}, the burned gas fraction and temperature of the gas in the exhaust runner after the blow down process b_{er} and T_{er}. In order to capture the thermal dynamics associated with an insulated exhaust runner, a first order lag with 3.6 sec (30 cycles) time constant τ_{er} is added to the temperature of the gas entering the exhaust runner, T_{er}. Thus the temperature of the gas that is re-inducted from the exhaust runner to the cylinder during re-breathing, T_{rbl} becomes the 9^{th} state.

$$\frac{d}{dt}T_{rbl} = \frac{1}{\tau_{er}}\left(T_{er} - T_{rbl}\right) \tag{1}$$

All the model equations can be found in the Appendix and for details please refer to [12].

Validation of the nine-state nonlinear model during fuel step changes (fixed RBL and EGR values) is shown in Fig. 2. The predicted start of combustion (SOC) and the predicted in-cylinder AFR are also shown in the second and third plot, respectively. For this open loop model validation we used a first order lag of 1.5 sec as the exhaust gas oxygen (EGO) sensor time constant.

The mean-value model captures the transients with reasonable accuracy without relying on detailed crankangle-resolved dynamics as in [9]. The controller synthesis and design detailed in Sec. IV is based on the mean-value model using the Linear Quadratic Gaussian (LQG) optimal control techniques on physical state-space representation of the system. Prior papers [14], [7] have shown promising results with LQ based control design. The authors in [14] design a state feedback controller based on LQ tuning approach. They demonstrate in simulations that during fixed fueling (propane) level, variable valve timing can successfully change the peak pressure while maintaining fixed combustion phasing. In [7] a LQ integral based controller was designed and experimentally tested for a dual fuel HCCI engine. The experimental tests were performed around the operating point where the open loop plant was identified. In this paper, physical interpretation of the system states is used for tuning the controller and observer gains in order to avoid high gain that can lead to sensitive and fragile implementation at operating points further away from the nominal operating point. Analysis of the multivariable controller in Sec. IV also indicates that the exhaust manifold filling, composition, and temperature dynamics are important for fast CA50 and AFR regulation during changes in gasoline fuel level. Note that AFR control was not explicitly considered in prior work [14], [7] and the simulations or experimental results are shown under air flow conditions that can only be achieved in a dynamometer facility.

Our model is discretized with sampling time being the engine cycle time τ and the control problem is defined as

$$\begin{aligned}
&x(k+1) = f(x(k),u(k),w(k)) \quad \text{Nonlinear State Equation}\\
&y(k) = f_y(x(k),u(k),w(k)) \quad \text{Nonlinear Output Equation}\\
&x = [m_1 \quad m_2 \quad b_1 \quad b_2 \quad p_2 \quad W_{c2} \quad b_{er} \quad T_{er} \quad T_{rbl}]^T\\
&u = [RBL \;\; EGR]^T \quad w = Fuel \quad y = [CA50 \;\; AFR_{ego}]^T.
\end{aligned}$$

III. Linear versus Nonlinear Open Loop Response

Linearization is performed around a fueling level W_f^{nom}=9 mg/cycle, and nominal control inputs RBL^{nom}=3.6 mm and EGR^{nom}=13 mm^2 such that the desired CA50$_{des}$=5.5^o and AFR$_{des}$=20 are achieved:

$$\begin{aligned}
\delta x(k+1) &= A\delta x(k) + B\delta u(k) + B_w\delta w(k)\\
\delta y(k) &= C\delta x(k) + D\delta u(k) + D_w\delta w(k).
\end{aligned} \tag{2}$$

Figure 3 shows the open loop responses of the linearized model and nonlinear model for Fuel, RBL and EGR steps. The simulation shows a fuel step from 9 to 10 mg/cycle at t=24 s and step-down back to the nominal fueling value 9 mg/cycle at t=48 s. Steps in RBL from 3.6 to 4 mm at t=72 s, from 4 to 3 mm at t=96 s, and back to the nominal value 3.6 mm at t=120 s are shown. Finally, one EGR step up from 13 to 20 mm^2 is shown in the last step at

t=144 s. The step responses indicate that RBL can affect both performance variables rapidly. The effects of RBL on the performance variables are similar to the effects of Fuel (disturbance) to the performance variables. The EGR actuator, on the other hand, affects the AFR but has weak effects on CA50.

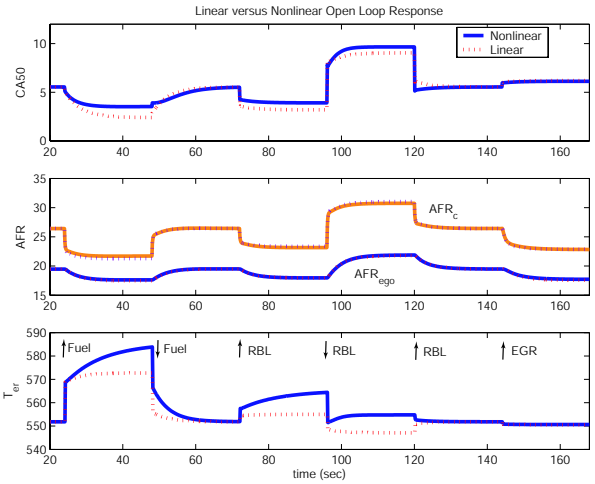

Fig. 3. Open loop response of the linearized and nonlinear model during step changes in all engine inputs.

The differences between the linear and the nonlinear response of the gas temperature in the exhaust runner T_{er} during an RBL step indicates that there exists a non-monotonic behavior between RBL and T_{er}. A non-monotonic behavior between an actuator and a state might deteriorate the closed loop response when linear control techniques are applied. This problem is addressed by the control design presented next. It is important also to note that the non-monotonic behavior is not coincidental but it is inherent to the TI engine. Further investigation using the nonlinear plant demonstrates that for a given fueling level there is a minimum T_{er} that can be achieved by varying RBL. By simple analogy to spark timing for SI engines, the RBL value that corresponds to the minimum T_{er} achieves the highest fuel economy because the chemical energy of the fuel is transformed to useful work instead of exhaust heat. The implications of the non-monotonic behavior to the thermal system stability are analyzed in [13].

IV. Control Analysis and Design

The TI engine controller shown in Fig. 4 is based on an integrator augmented state feedback and an observer using linear optimal techniques. Although the control design approach is standard, a few steps required carefull analysis and tuning. The linearized model is first normalized: each state is normalized with its own nominal value and the inputs and outputs are scaled with proper physical units. Grammian-based balanced realization is then applied to identify the modes that are weakly controllable and/or observable. In particular, if the controllability and observability grammians of (2) are G_c and G_o, the state coordinate transformation

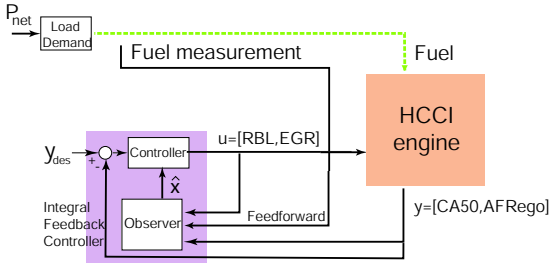

Fig. 4. The control structure for a HCCI engine.

$\delta\bar{x} = T\delta x$ produces the equivalent model and transforms the grammians to $\bar{G}_c = TG_cT^T$ and $\bar{G}_o = T^{-T}G_oT^{-1}$.

The balanced realization computes a particular similarity transformation T such that

$$\bar{G}_c = \bar{G}_o = diag(g) = \begin{bmatrix} g_1 & 0 & \dots & 0 \\ 0 & g_2 & \dots & 0 \\ \vdots & & \ddots & \vdots \\ 0 & \dots & 0 & g_9 \end{bmatrix}. \quad (3)$$

Table I shows the vector g and the state similarity transformation matrix T. If the system is normalized properly, the computation of g can be used to reduce the model order. Specifically, the individual elements of g reflect the combined controllability and observability of individual states of the balanced model. The states corresponding to a small value in g can be deleted without significant effects to the input-output characteristics of the original system. Table I indicates that the last three states of the transformed system can be eliminated. Through the transformation matrix T, we then find the states in the original system that have the least influence on the input-output behavior. After balanced realization most of the dynamics depend on the three exhaust manifold states, m_2, b_2, and p_2 and the temperature of the gas re-inducted from the exhaust runner T_{rbl}.

TABLE I

The similarity transformation matrix (T) and vector of the diagonal of the balanced gramian (g).

T									g
m_1	m_2	b_1	b_2	p_2	W_{c2}	b_{er}	T_{er}	T_{rbl}	
-2.35	-27.18	-4.35	-116.97	0.13	-2.17	-9.53	-6.99	-205.43	3
1.49	-9.72	3.02	73.69	7.1	-1.68	6.12	-24.64	-724.45	1.23
-3.84	-60.36	-7.24	35.46	14.89	-2.24	-1.13	-5.1	-149.8	0.24
1.53	12.64	0.49	5.41	31.91	29.32	-0.64	0.55	16.05	0.14
-0.09	180.37	0.43	2.03	-135.43	7.38	-3.7	4.32	127.05	0.03
-0.03	2.68	-1.55	-2.06	16.67	17.67	7.53	-0.55	-16.24	0.03
0.13	-0.24	0.04	-0.09	12.89	-0.19	0.04	-0.01	-0.27	0
0	0	0	0	0.03	0	0	0	0	0
0.08	0	0	0	0.06	0	0	0	0	0

The knowledge of the important states is used to tune the observer gain L and thus the error convergence of the variables that matter for control. The observer state equations are

$$\begin{aligned} \delta\hat{x}(k+1) &= A\delta\hat{x}(k) + B\delta u(k) + B_w\delta w(k) \\ &+ L(\delta y(k) - \delta\hat{y}(k)) \\ \delta\hat{y}(k) &= C\delta\hat{x}(k) + D\delta u(k) + D_w\delta w(k). \end{aligned} \quad (4)$$

The optimal observer gain L can be solved based on the Linear Quadratic Gaussian method: $L = APC^T(W + CPC^T)^{-1}$ with $P = V + APA^T - APC^T(W + CPC^T)^{-1}CPA$. The positive definite matrices V and W represent the intensities of the process disturbance and measurement noise respectively.

Based on the banlanced realization results higher weighting is assigned to the elements in V corresponding to the states m_2, b_2, p_2, and T_{rbl} whereas the elements in V corresponding to m_1, b_1, b_{er}, and T_{er} are given very small weighting since those states are almost unobservable and uncontrolable based on the balanced realization. De-emphasizing T_{er} in the observer design alleviates any problems that might have occurred due to the non-monotonic behavior of RBL to T_{er}.

Based on the separation principle the LQG controller is completed with a state feedback. Integral control is used together with state feedback to reduce the steady-state error of the control input. The state equations of the augmented states $q(k)$ represent the integral of the difference between the reference input y_{des} and the output $y(k)$: $q(k+1) = q(k) + \tau(\delta y_{des} - \delta y(k))$. The control law is then: $u(k) = -K\delta\hat{x}(k) - K_I q(k)$ where $\delta\hat{x}(k)$ is the estimate of the state determined using a state observer in (4) and K and K_I are the controller gains computed using the LQR method.

The block diagram of the LQG controller and plant is shown in Fig. 5. The block diagram shows the transfer functions from the actuators *RBL* and *EGR* and the measurable fuel disturbance *FUEL* to the performance variables *CA*50 and *AFR* which can be derived from the state equations (2):

$$\begin{bmatrix} CA50 \\ AFR \end{bmatrix} = \begin{bmatrix} G_{11} & G_{12} & G_{13} \\ G_{21} & G_{22} & G_{23} \end{bmatrix} \begin{bmatrix} RBL \\ EGR \\ FUEL \end{bmatrix}. \tag{5}$$

The LQG controller (C_{LQG}) contains the dynamic feedforward terms from the measurable fuel disturbance *FUEL* to the actuators *RBL* and *EGR* (C_{w1} and C_{w2}) and the feedback from the measurement *CA*50 and *AFR* to the actuators *RBL* and *EGR* (C_{11}, C_{12}, C_{21} and C_{22}):

$$\begin{bmatrix} RBL \\ EGR \end{bmatrix} = \underbrace{\begin{bmatrix} C_{11} & C_{12} & C_{w1} \\ C_{21} & C_{22} & C_{w2} \end{bmatrix}}_{C_{LQG}} \begin{bmatrix} CA50 \\ AFR \\ FUEL \end{bmatrix} \tag{6}$$

where the transfer functions of the controller are given by

$$\begin{aligned} C &= \begin{bmatrix} C_{11} & C_{12} \\ C_{21} & C_{22} \end{bmatrix} = \left(K(zI - A + BK)^{-1}B - I\right) K_I \frac{\tau}{z-1} \\ C_w &= \begin{bmatrix} C_{w1} \\ C_{w2} \end{bmatrix} = -K\left((zI - A + BK)^{-1}B_w\right). \end{aligned} \tag{7}$$

Note that the transfer function C from $\delta y_{des} - \delta y$ to δu and C_w from δw to δu are both independent of the observer gain L because the error state $\tilde{x}(k) = \delta x(k) - \delta\hat{x}(k)$ is uncontrollable from the input $\delta y_{des} - \delta y$ or the disturbance $\delta w(k)$.

V. Control Results

First we assume perfect measurements of both performance variables. The closed loop performance in regulating CA50 and AFR during fuel step changes (9-10-9-8-9 mg/cycle) is demonstrated in Fig. 6. If RBL and EGR are held fixed, the open loop response of CA50 and AFR deviates significantly from the desired values as shown with the dashed line in Fig. 6. The closed loop response is shown with the solid line in Fig. 6. Note that the EGR participation during the fuel steps is transient and has minimal effects during steady state. The controller achieved regulation even during large fuel steps from 7 to 11 mg/cycle demonstrating a reasonable level of robustness.

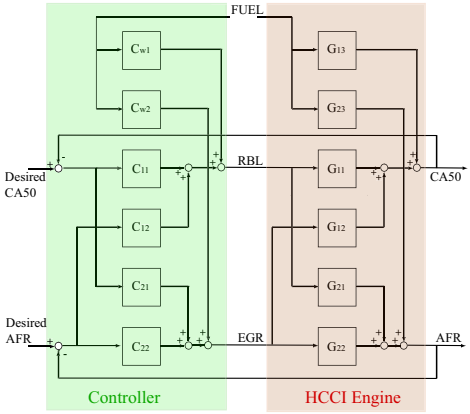

Fig. 5. Block diagram of the TI engine plant and LQG controller

In reality, the cycle-to-cycle variability in combustion introduces noise in the CA50 measurement as shown in Fig. 2. We thus investigate the effect of measurement noise on the regulation results by adding ± 1 degree uniform random number noise in the *CA*50 measurement. Fig 7 shows surprisingly that there is no degradation of performance for noisy measurements. The success of the controller despite measurement noise can be explained by looking at the structure of the controller from the block diagram of the LQG controller and plant in Fig. 5. As can be seen from the Bode magnitude plots of the feedforward and feedback part of the controller in Fig. 8, the LQG controller relies largely on the feedforward part, especially from FUEL to RBL (C_{w1}). The feedback part can be approximated by integrators. Thus the measurement noise in *CA*50 does not affect the closed loop performance because it is averaged from the feedback integral controller. As long as the feedforward is accurate, the LQG controller achieves good disturbance rejection. To facilitate implementation on a dynamometer facility, an equivalent reduced order controller is derived in the next section.

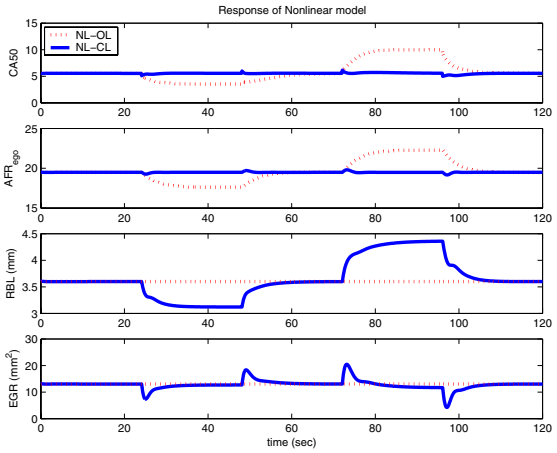

Fig. 6. Open-loop and closed-loop response (without measurement noise)

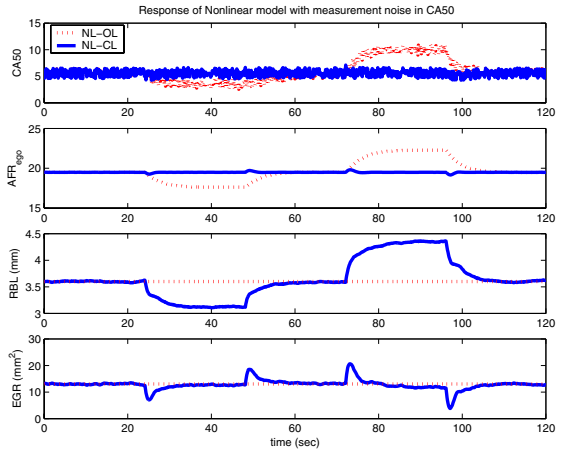

Fig. 7. Open-loop and closed-loop response (with measurement noise)

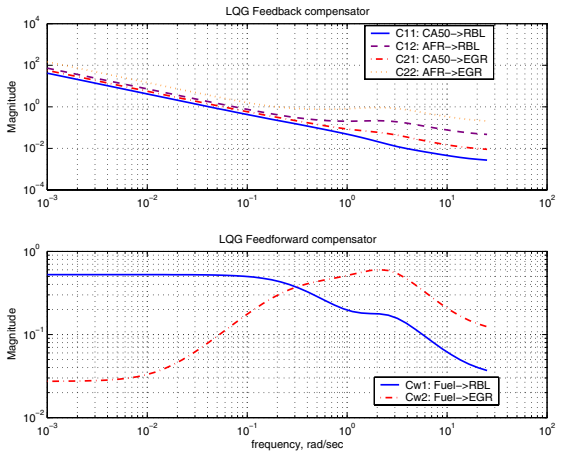

Fig. 8. Bode magnitude plot of the feedback and feedforward controller

VI. Controller Simplification for Implementation

The feedforward (C_{w1} and C_{w2}) terms of the LQG controller are both nine-order filters and each feedback (C_{11}, C_{12}, C_{21} and C_{22}) term is an eleven-order filter. From the actuator authority analysis in Sec. III it is possible to infer that RBL is faster and stronger actuator to regulate $CA50$ than the other actuator EGR. Whereas, EGR is strong enough to regulate AFR. Thus, our first step is to eliminate the cross coupling terms C_{12} and C_{21} in Fig. 5 investigating if a decentralized feedback can handle the interactions. The decentralized feedback controller C_{dec} with the off diagonal feedback C_{12} and C_{21} set to zero

$$\begin{bmatrix} RBL \\ EGR \end{bmatrix} = \underbrace{\begin{bmatrix} C_{11} & 0 & C_{w1} \\ 0 & C_{22} & C_{w2} \end{bmatrix}}_{C_{dec}} \begin{bmatrix} CA50 \\ AFR \\ FUEL \end{bmatrix}. \tag{8}$$

is compared with the fully multivariable controller C_{LQG}. The simulation results shown in Fig. 10 indicate that the C_{12} and C_{21} terms do not contribute significantly and thus can be eliminated. Further simplification is possible by examining the frequency plot of the gain of C_{w2}. Specifically, the Bode plot in Fig. 8 shows that the feedforward from $Fuel$ to EGR (C_{w2}) has little effect at low frequencies. In addition, the control response in Fig. 6 and Fig. 7 show that EGR is active during transients with small deviation in steady state. Thus, we further eliminate C_{w2}. We, then, replace C_{w1} with a cancelation feedforward conroller $C_{uw} = -G_{11}^{-1}G_{13}$. The plant transfer function G_{11} and G_{13} are derived from the reduced order model based on balanced realization and do not require LQG control design, exploiting the fact that RBL is a strong actuator that can eliminate the fuel disturbance on CA50. Further investigation of the Bode plot in Fig. 8 allows the approximation of the feedback C_{11} and C_{22} terms with two integrators as shown in Fig. 9. Thus the cancelation feedforward with integral feedback controller C_{red} is a reduced equivalent controller:

$$\begin{bmatrix} RBL \\ EGR \end{bmatrix} = \underbrace{\begin{bmatrix} \frac{-0.12}{s} & 0 & C_{uw} \\ 0 & \frac{-0.0428}{s} & 0 \end{bmatrix}}_{C_{red}} \begin{bmatrix} CA50 \\ AFR \\ FUEL \end{bmatrix}. \tag{9}$$

Figure 10 presents the closed loop responses of the plant with (i) the full order LQG controller C_{LQG}, (ii) the decentralized feedback controller C_{dec} and (iii) the cancelation feedforward with integral feedback C_{red}. The cancelation feedforward with integral feedback (C_{red}) is the simplest controller we can derive before sever degradation. The feedforward C_{uw} from Fuel to RBL is a five-order controller and the feedback consists of two integrators. Thus, the proposed controller compensate for the exhaust manifold and runner dynamics and is higher order than the 2nd order LQG controller proposed in [14].

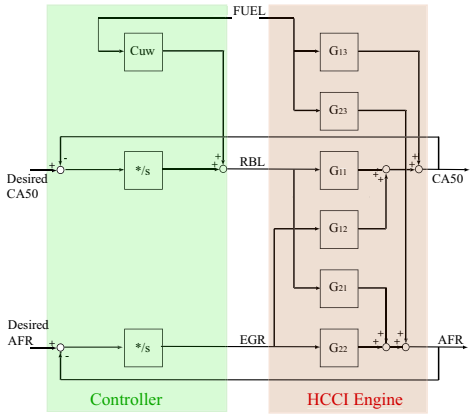

Fig. 9. Block diagram of the TI engine plant with cancellation feedforward and integral feedback decentralized control.

VII. Conclusion

In this paper we design a multivariable controller that manages RBL and EGR actuators to regulate CA50 and AFR during fuel load transients. We then reverse engineer the multivariable controller and simplify it to decentralized feedback and a disturbance decoupler. The simplification is possible due to the weak interaction between the performance variables. Indeed, in our combustion model CA50 depends primarily on the charge temperature and not charge

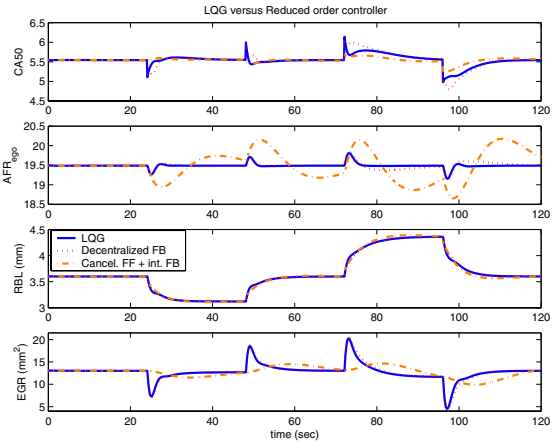

Fig. 10. Closed loop simulation results of the plant with (i) the full order LQG controller (solid line), (ii) the decentralized feedback controller (dotted line) and (iii) the cancelation feedforward with integral feedback controller (dashed line)

composition (cylinder AFR). Moreover, most of the dynamics (after balanced realization) depend on the exhaust manifold states (m_2, b_2, and p_2) and the filtered temperature in the exhaust manifold T_{rbl}. The *RBL* controller can be a slow controller that cancels the slow temperature dynamics in the exhaust runner thus the temperature dynamics need to be identified very well. Heat transfer and the interactions among (i) the cooling loop, (ii) the wall temperature, and (iii) the temperature of the rebreathed flow T_{rbl} need to be represented if a model-based control design (including slow pole cancelation) is desirable.

The reason that EGR is not necessary for the AFR control of the TI engine is as follows. When our controller decreases RBL during an increase in fuel, it increases the fresh air in the cylinder, which balances the AFR despite the fuel increase. Therefore, the RBL controller handles both CA50 and AFR regulation for the most part. In steady-state, EGR is minimally used to adjust any remaining error in AFR, and thus an integral controller would suffice.

ACKNOWLEDGMENT

This work is funded by the General Motors Corporation. We thank J.-M. Kang, C.-F. Chang, and M.-F Chang of General Motors Corporation for the experimental data and J. S. Freudenberg from the University of Michigan for his advice on the control design.

APPENDIX

The 9 state equations are denoted by $*$.

$$* \quad \frac{d}{dt}m_1 = W_{01} + W_{21} - W_{1c}; \quad p_1 = m_1 R T_1 / V_1$$
$$* \quad \frac{d}{dt}b_1 = \left[-W_{01} i_1 + W_{21}(b_2 - b_1)\right]/m_1$$
$$* \quad \frac{d}{dt}m_2 = W_{c2} - W_{20} - W_{21} - W_{2c}$$
$$* \quad \frac{d}{dt}b_2 = \left[W_{c2}(b_{er} - b_2)\right]/m_2$$
$$* \quad \frac{d}{dt}p_2 = \gamma R\left(W_{c2}\tilde{T}_{er} - (W_{20} + W_{21} + W_{2c})T_2\right)/V_2$$
$$\text{where} \quad \tilde{T}_{er} = T_{rbl} - \Delta T_{er2}; \quad T_2 = p_2 V_2/(R m_2)$$
$$* \quad W_{c2}(t+\tau) = W_{1c}(t) + W_f(t) + W_{2c}(t)$$
$$* \quad T_{er}(t+\tau) = T_{bd}(t)$$
$$* \quad b_{er}(t+\tau) = b_{bd}(t) \quad \text{where} \quad \tau = N/120$$

$$* \quad \frac{d}{dt}T_{rbl} = \left(T_{er} - T_{rbl}\right)/\tau_{er}$$
$$p_{ivc} = \beta_0 + \beta_1 p_1$$
$$W_{1c} = (1 - x_r)m_c/\tau - W_f; \quad W_{2c} = \frac{x_r}{\tau} m_c$$
$$x_r = \alpha_1\left(1 + \kappa_0 \frac{p_1^{\kappa_1}}{p_2^{\kappa_2}\sqrt{T_{rbl}}}\right)\underbrace{\left(u_{rbl} + \alpha_2 u_{rbl}^2 + \alpha_3 u_{rbl}^3\right)}_{C_d A_{rbl}}$$
$$T_{ivc} = T_1(1 - x_r) + T_{rbl} x_r; \quad m_c = p_{ivc} V_{ivc}/(R T_{ivc})$$
$$b_c = (1 - x_r)\frac{W_{1c}}{W_{1c} + W_f} b_1 + x_r b_{er}$$
$$b_{bd} = \frac{AFR_s + 1}{AFR_c + 1}(1 - b_c) + b_c$$
$$AFR_c = \left[(1 - b_1)W_{1c} + (1 - b_{er})W_{2c}\right]/W_f$$
$$AFR_2 = (1 - b_2 + AFR_s)/b_2$$
$$\int_{\theta_{ivc}}^{\theta_{soc}} A p_{ivc}^n v_{ivc}^{n_c n}(\vartheta) exp\left(-\frac{E_a v_{ivc}^{1-n_c}(\vartheta)}{R T_{ivc}}\right) d\vartheta = 1$$
$$\text{with} \quad v_x(\vartheta_y) = V_c(\vartheta_x)/V_c(\vartheta_y)$$
$$T_{soc} = T_{ivc} v_{ivc}^{(n_c - 1)}(\theta_{soc}); \quad \theta_c = \theta_{soc} + \Delta\theta$$
$$\text{where} \quad \Delta\theta = k\left(T_{soc}\right)^{(-2/3)}\left(T_m\right)^{1/3} exp\left(\frac{E_c}{3 R_u T_m}\right)$$
$$T_m = T_{soc} + e\Delta T; \quad \Delta T = Q_{LHV} m_f/\left(c_v m_c\right)$$
$$e = a_0 + a_1 k; \quad k = b_0 + b_1\theta_{soc} + b_2\theta_{soc}^2$$
$$\theta_{CA50} = \theta_{soc} + .55\Delta\theta$$
$$T_{bc} = T_{ivc} v_{ivc}^{(n_c - 1)}(\theta_c); \quad p_{bc} = p_{ivc} v_{ivc}^{n_c}(\theta_c)$$
$$T_{ac} = T_{bc} + (1 - b_c)\Delta T \quad \text{and} \quad p_{ac} = p_{bc} T_{ac}/T_{bc}$$
$$T_{evo} = T_{ac} v_c^{(n_e - 1)}(\theta_{evo}) \quad \text{and} \quad p_{evo} = p_{ac} v_c^{n_e}(\theta_{evo})$$
$$T_{bd} = T_{evo}\left(p_2/p_{evo}\right)^{(n_e - 1)/n_e} + \Delta T_{bd}$$

REFERENCES

[1] J. Willand, R.-G. Nieberding, G. Vent, and C. Enderle, "The knocking syndrome - its cure and its potential," *SAE paper 982483*.

[2] J. Chen and W. Stevens, "Autoignition and control of flameless combustion," Department of Energy, Tech. Rep., August 2002.

[3] J. Yang, T. Culp, and T. Kenney, "Development of a gasoline engine system using hcci technology - the concept and the test results," *SAE paper 2002-01-2832*.

[4] G. Haraldsson, P. Tunestal, and B. Johansson, "HCCI combustion phasing in a multi cylinder engine using variable compression ratio," *SAE paper 2002-01-2858*.

[5] D. S. Stanglmaier and E. Roberts, "Homogenous charge compression ignition (HCCI): Benefits, compromises, and future engine applications," *SAE paper 1999-01-3682*.

[6] J. O. Olsson, P. Tunestal, and B. Johansson, "Closed loop control of an HCCI engine," *SAE paper 2001-01-1031*.

[7] J. Bengtsson, P. Strandh, R. Johansson, P. Tunestal, and B. Johansson, "Cycle-to-cycle control of a dual-fuel HCCI engine," *SAE paper 2004-01-0941*.

[8] J. A. Souder, "Control of multi-cylinder HCCI engine," *SAE Homogeneous Charge Compression Ignition Symposium 2004*.

[9] G. Shaver, J. Gerdes, P. Jain, P. Caton, and C. Edwards, "Modeling for control of HCCI engines," in *Proc. of the American Control Conf.*, 2003, pp. 749–754.

[10] P. Najt and D. Foster, "Compression-ignited homegeneous charge combustion," *SAE paper 830264*.

[11] R. H. Thring, "Homegeneous-charge compression-ignition (HCCI) engines," *SAE paper 892068*.

[12] D. J. Rausen, A. G. Stefanopoulou, J.-M. Kang, J. A. Eng, and T.-W. Kuo, "A mean-value model for control of homogeneous charge compression ignition (HCCI) engines," in *Proc. of the American Control Conf.*, 2004, pp. 125–131, (Also appear in ASME Journal of Dynamic Systems, Measurement, and Control).

[13] C. J. Chiang and A. G. Stefanopoulou, "Steady-state multiplicity and stability of thermal equilibria in homogeneous charge compression ignition (HCCI) engines," *43rd IEEE Conference on Decision and Control (CDC 2004)*.

[14] G. Shaver and J. Gerdes, "Cycle-to-cycle control of HCCI engines," *2003 ASME Proc. of International Mechanical Engineering Congress and Exposition IMECE2003-41966*.